Magnetic structure and phase transition in a single crystal of $ErCrO_3$

S. Yano,[1] Chin-Wei Wang,[1] Yinghao Zhu,[2] Kaitong Sun,[2] and Hai-Feng Li[2]
[1]*National Synchrotron Radiation Research Center, Hsinchu 30077, Taiwan*
[2]*Joint Key Laboratory of the Ministry of Education, Institute of Applied Physics and Materials Engineering, University of Macau, Avenida da Universidade, Taipa, Macao SAR 999078, China*

(Received 11 December 2022; revised 28 September 2023; accepted 12 October 2023; published 2 November 2023)

We investigated the magnetic phase transitions of $ErCrO_3$ using single-crystal and powder samples. Neutron powder diffraction showed that the Cr^{3+} orders at $T_N = 133$ K with the irreducible representation of Γ_4 (G_x, F_z). $ErCrO_3$ exhibits a mixed Γ_4 $(G_x; F_z^R)$ and Γ_1 $(G_y; C_z^R)$ phase just below 10 K. The Γ_1 $(G_y; C_z^R)$ phase becomes dominate at the base temperature. On the other hand, the transition from Γ_4 (G_x, F_z) to Γ_1 $(G_y; C_z^R)$ is sharp in the single-crystal sample. The scattered intensity of the (110) Bragg peak, which indicates the ferromagnetic component along the c axis, displays continuous growth upon cooling and dropped starting at $T_{SR} = 9.6$ K when the spin reorientation of Cr^{3+} occurs. The temperature-dependent magnetization measurement of the single-crystal sample showed the ferromagnetic moment is along the c axis appearing at $T_N \approx 133$ K with a sharp drop at $T_{Er^{3+}} = 10$ K. The specific heat shows a sharp peak at $T_{Er^{3+}} = 9.3$ K for the single crystal while the polycrystalline sample does not. The crystal-field excitation of the first Kramers doublet above the ground state of $^4I_{15/2}$ of Er^{3+} is observed at $\approx$1.19(1) meV (=13.80 K), which is close to the Schottky anomaly observed as $\Delta = 13.23$ K from the lowest-lying crystal-field states in the specific heat. It is not yet clear whether the near coincidence of T_{SR} and $T_{Er^{3+}}$ is an accident or not.

DOI: 10.1103/PhysRevB.108.174406

I. INTRODUCTION

Perovskite oxides have been a focus of attention following the discoveries of high-temperature superconductivity in cuprates, colossal magnetoresistance in manganites, and room-temperature magnetically induced ferroelectricity in orthoferrites [1–3]. Because of these promising applications, the materials have been studied for decades.

Among the perovskite materials, the rare-earth orthochromites $RCrO_3$ and orthoferrites $RFeO_3$ share many similarities. Both families of compounds crystallize in the centrosymmetric space group *Pbnm* (No. 62) [4]. The R^{3+} and (Cr or Fe)$^{3+}$ are magnetic atoms that occupy the 4*c* and 4*b* positions, respectively. The structure leads to the emergence of antiferromagnetic and weak ferromagnetic ordering of Cr^{3+} at $T_N^{Cr} = 110$–280 [5] and in orthoferrites $RFeO_3$ at $T_N^{Fe} = 620$–740 K [6]. Some of them show spin reorientation at the $T_{SR}^{Cr,\,Fe}$. The symmetry of magnetic orders of (Fe, Cr)$^{3+}$ is Γ_1 (A_x, G_y, C_z) or Γ_2 (F_x, A_y, G_z), or Γ_4 (G_x, A_y, F_z). The R^{3+} shows antiferromagnetic order at the lower temperatures ($T_{R^{3+}}$) which are typically several K [6]. Magnetic order of the rare-earth sublattice of $RFeO_3$ only appears at temperatures lower than T_{SR}. That means the spin reorientation is not simply related to ordering of the rare-earth moment for $RFeO_3$. On the other hand, these T_{SR} and $T_{R^{3+}}$ are closer in the orthochromites $RCrO_3$ (R = Y, Ho, Er, Yb, Lu). Here in the rare-earth orthochromites and orthoferrites, magnetic interactions R^{3+}-R^{3+}, R^{3+}-(Cr, Fe)$^{3+}$, and (Cr, Fe)$^{3+}$-(Cr, Fe)$^{3+}$ can coexist and establish a variety of magnetic structures and phase transitions.

In the rare-earth orthochromites $RCrO_3$ with nonmagnetic R = (Lu, Y, and La) show no spin-reorientation [7] so the magnetic interaction between enhanced R^{3+} and Cr^{3+} is the key to understanding the physics of $RCrO_3$. The field switchable polarization occurs in the rare-earth orthochromites only when R is magnetic and they are in the weak ferromagnetic phase of Cr^{3+} below T_{SR}^{Cr}. $RCrO_3$ has received much interest for applications, such as an electrode material [8], interconnector for solid-state fuel cells [9], and magnetocaloric effect for refrigeration [10].

Here, we focus attention on $ErCrO_3$. $ErCrO_3$ crystallizes in centrosymmetric space group *Pbnm* (No. 62) at room temperature like other $RCrO_3$. $ErCrO_3$ is the only material in the orthochromites that show spin reorientation of Cr^{3+} ions from Γ_4 (G_x, A_y, F_z) to Γ_1 (A_x, G_y, C_z) transition with the magnetic rare-earth R in the orthochromites [11]. So there are three transitions; antiferromagnetic order of Cr^{3+} at $T_N \approx$ 133 K, the spin reorientation of Cr^{3+} from Γ_4 $(G_x, A_y, F_z; -)$ to Γ_1 $(A_x, G_y, C_z; -)$ at $T_{SR} \approx 10$–20 K, and antiferromagnetic order of Er^{3+} with Γ_1 $(A_x, G_y, C_z; -C_z^R)$ at $T_{Er^{3+}} \approx 6$–10 K.

However, the reported values of T_{SR} and $T_{Er^{3+}}$ are not consistent. For example, magnetization measurements on a polycrystalline sample report $T_{SR} = 22$ K [12,13], magnetization measurements of single-crystal samples give $T_{SR1} =$ 10.2 K and $T_{SR2} = 6.0$ K [14], $T_{SR} = 9.8$ K [15], $T_{SR} = 9.7$ K [16], and optical observation with single-crystal samples $T_{SR} = 9.8$ K [17], $T_{SR} = 9.4$ K [18,19], or $T_{SR} = 9.3$ K [20]. The reported values of the transition temperature of Er^{3+} also vary, with magnetization data showing $T_{Er^{3+}} = 6.5$ K [12] and neutron diffraction showing $T_{Er^{3+}} = 16.8$ K [21]. Sometimes, they are reported as $T_{SR} = T_{Er^{3+}}$. The Er^{3+} ions, whose ground state is $^4I_{15/2}$, have a large saturation magnetic

moment of 9 μ_B or larger with a large orbital contribution [16,22]. The specific-heat data also shows that a sharp transition occurs at $T = 9.82$ K in addition to a Schottky anomaly [23].

These transition temperatures are critical for controlling the magnetic phase. For example, the Γ_4 state can be recovered from the Γ_1 state by applying an external field along the c axis. This field-induced spin reorientation takes place at about 1.0 kOe at 1.5 K [24]. The specific-heat measurement showed that an external magnetic field of 9.2 kOe could suppress the spin reorientation [23]. Pulsed laser irradiation induces magnetic phase transitions of the $ErCrO_3$ [25]. Interestingly, the time necessary for completing the phase transition is 0.7 μs when Er^{3+} in the antiferromagnetic phase is selectively excited by the tunable dye laser, in contrast with 0.4 μs when Cr^{3+} are excited by a ruby laser. This is because if Cr^{3+} ions are excited, Cr^{3+} rises at first by the Cr^{3+}-Cr^{3+} magnetic interaction, then energy of Cr^{3+} spin system flows to the Er^{3+} so the Er^{3+} rises. On the other hand, when the Er^{3+} ions are selectively excited, because Er^{3+}-Er^{3+} interaction is two orders of magnitude smaller than that of the Cr^{3+}-Cr^{3+}, the energy flows from the spin state of the excited Er^{3+} to Cr^{3+} ions by the Cr^{3+}-Er^{3+} interaction first. Then, the system spreads the energy of Cr^{3+} via the Cr^{3+}-Cr^{3+} interaction. Finally, their thermal equilibrium was achieved by Cr^{3+}-Er^{3+} in the second time.

The multiferroic properties have been investigated for $RCrO_3$ [13,22,26,27]. Although the field-induced polarization reversal behavior on the polycrystalline sample of $RCrO_3$ (R = Sm, Gd, Er, and Lu), the uniform ferroelectric ordering in the temperature range of 5–370 K was not found in single-crystal $ErCrO_3$ in any of the crystal directions. Either controlling these phases via temperature, magnetic field, electric field, or laser, to clarify the magnetic phase transition of $ErCrO_3$ in detail should be an important step. Here, we have utilized various experimental techniques to study $ErCrO_3$ to clarify these magnetic phase-transition temperatures.

II. EXPERIMENT

The single crystals of $ErCrO_3$ were grown in a well-equipped laser-diode floating-zone furnace (Model: LD-FZ-5-200W-VPO-PC-UM) at the University of Macau, Macao, China. The polycrystalline sample of $ErCrO_3$ was pulverized from the single-crystal sample. We carefully selected and gently ground an $ErCrO_3$ single crystal into a powdered sample with a vibratory micromill (Fritsch Pulverisette 0) for the neutron-scattering study, to determine the temperature-dependent crystal and magnetic structures. The measurements of DC magnetization and specific heat were carried out using the vibrating sample magnetometer and heat-capacity options on a Quantum Design physical property measurement system (PPMS DynaCool instrument). To perform magnetization measurements with magnetic fields parallelling to the a, b, and c crystallographic axes, an as-grown $ErCrO_3$ single crystal was aligned with an in-house x-ray Laue diffractometer. The aligned single-crystal sample was then glued to a quartz sample holder with GE varnish. The DC magnetization at an applied magnetic field of 100 Oe was measured with the zero-field cooling (ZFC) and field cooling (FC) modes at 2–350 K. Magnetic hysteresis loops from 14 to −14 T and then back to 14 T were measured at 3, 6, 15, and 300 K. The specific heat was measured with a thermal relaxation method, which measures the relaxation time of the heat flux from specimen to a thermal bath. Neutron powder diffraction (NPD) experiments were conducted on the high-resolution powder diffractometer, Echidna [28] located at the OPAL reactor at the Australian Centre for Neutron Scattering (ACNS) in the Australian Nuclear Science and Technology (ANSTO). The neutron wavelength of 2.4395 Å defined by Ge (331) crystals at 140° take-off angle was used. For single-crystal measurement, the weight of the sample was 0.67 g and aligned in the ($h0l$) plane and ($0kl$). Neutron-scattering data were collected at Sika at ACNS in ANSTO [29]. The collimations were open-60′-60′-60′or open-open-60′-60′ with E_f fixed = 5 meV. The cooled Be filter was placed on the scattering side to cut off the higher-order wavelength contamination.

TABLE I. Atomic parameters determined by neutron powder diffraction experiment at $T = 300$ K. The $R_{\text{nuclear}} = 5.42\%$ with $\chi^2 = 1.77$.

Atom		x	y	z	Occ.	B
Er	4c	−0.0194(4)	0.0685(3)	0.25	1	0.198
Cr	4b	0.5	0	0	1	0.340
O1	4c	0.1061(4)	0.4629(4)	0.25	1	0.212
O2	8d	0.6929(3)	0.3012(3)	0.05456(2)	1	0.154

III. NEUTRON POWDER DIFFRACTION STUDY OF $ErCrO_3$

We have studied magnetic structures using pulverized samples. The crystal structures are determined as $Pbnm$ symmetry (No. 62) at all temperatures below 300 K. The neutron powder diffraction shows that the sample is a single phase, and the structure has been refined in $Pbnm$ with $a = 5.2226(2)$ Å, $b = 5.5162(2)$ Å, $c = 7.5192(3)$ Å at 300 K (Table I). By following Shamir's [5] notation, magnetic structures are summarized in Table II. Here, the magnetic structures are G-type{+, −, +, −}, A-type{+, −, −, +}, C-type{+, +, −, −}, and F-type{+, +, +, +} for {Cr(1), Cr(2), Cr(3), Cr(4)} and {Er(1), Er(2), Er(3), Er(4)} in Tables III to V. Figure 1 shows the four phases of $ErCrO_3$. At the lowest temperature of 5 K, the diffraction pattern shows clear (100) and (010) magnetic peaks where there is no nuclear peak from the crystal structure

TABLE II. Magnetic space group for each magnetic structure models. These magnetic structures are described as G-type{+, −, +, −}, A-type{+, −, −, +}, C-type{+, +, −, −}, and F-type{+, +, +, +} for {Cr(1), Cr(2), Cr(3), Cr(4)} and {Er(1), Er(2), Er(3), Er(4)} in Tables III to V.

Magnetic space group	Irrep	Cr			Er		
$Pbnm$	Γ_1	A_x	G_y	C_z			C_z^{Er}
$Pbn'm'$	Γ_2	F_x	C_y	G_z	F_x^{Er}	C_y^{Er}	
$Pb'nm'$	Γ_3	C_x	F_y	A_z	C_x^{Er}	F_y^{Er}	
$Pb'n'm$	Γ_4	G_x	A_y	F_z			F_z^{Er}

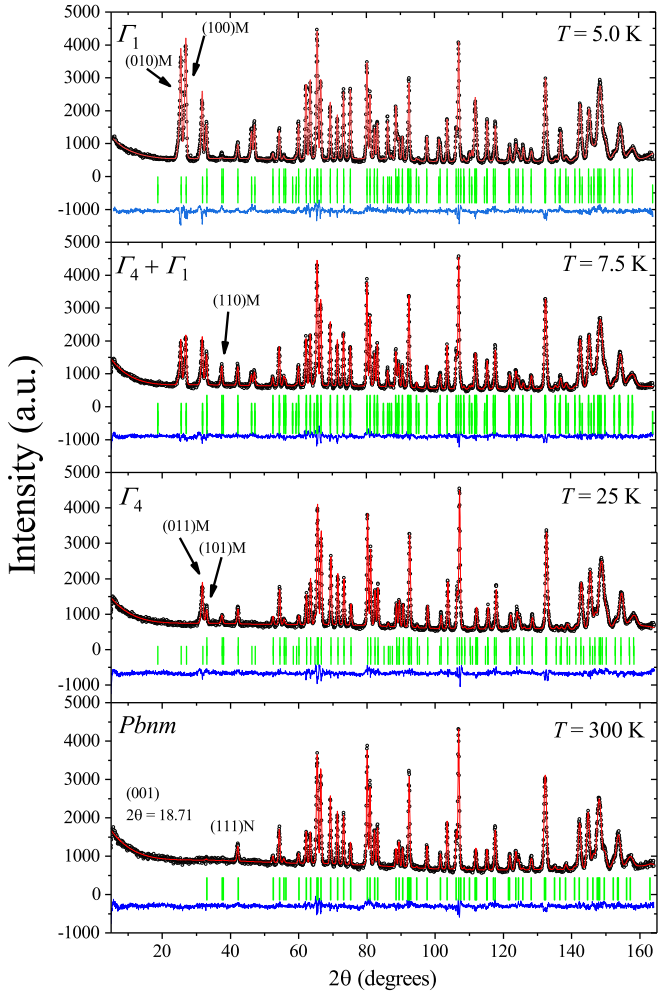

FIG. 1. Neutron powder diffraction patterns collected at $T = 5$, 7.5, 25, and 300 K.

of $ErCrO_3$ with *Pbnm* symmetry. The Γ_1 $(A_x, G_y, C_z; C_z^{Er})$ magnetic structure accounts for all the peaks in that phase shown in Fig. 2 on the left. The magnetic moments determined were shown in Table III with *R*-factors. If we add a small mixture of Γ_4 $(G_x, A_y, F_z; F_z^{Er})$ to Γ_1 $(A_x, G_y, C_z; C_z^{Er})$, χ^2 and *R*-factors slightly improve. The symmetry allows us to have magnetic component in these directions however the magnetic moments along the x and z for Cr were too small and within the error. So, finally it is determined as Γ_1 $(G_y; C_z^{Er})$. Our result is consistent with Bertaut's [21] but not with Shamir's [5]. Our calculation and single crystal diffraction data shown in the later section were consistent. The strong magnetic peaks (100) and (010) indicate that the Er^{3+} magnetic order contributes to the peak intensities as shown in Fig. 1. On the other hand, these peaks completely disappear at $T = 25$ K. For that phase, only Cr^{3+} orders with the symmetry Γ_4 (G_x, F_z) indexing all these peaks well as shown in Table V and Fig. 2 on the right. The magnetic moments determined were shown in Table V with *R*-factors. So far the previous works suggested spin reorientation from Γ_4 $(G_x, A_y, F_z; F_z^{Er})$ to Γ_1 $(A_x, G_y, C_z; -C_z^{Er})$. Our study shows that the transition observed here is continuous and from Γ_4 (G_x, F_z) to Γ_1 $(G_y; C_z^{Er})$. A interesting phase is at 7.5 K. The phase can be described as a mixture of Γ_4 (G_x, F_z^{Er}) phase and Γ_1 $(G_y; C_z^{Er})$ phase as summarized in Table IV. One can think of Cr^{3+} ferromagnetic component should exist instead of Er^{3+} ferromagnetic component however the model failed to fit the (110) peak. The magnetic peak of (110) is a representative peak that gradually grows below T_N, it increases the intensity below 10 K, and then suddenly decreases the intensity while cooling further. Table VI shows the calculation of nuclear and magnetic Bragg peaks based on the magnetic structure models shown above. The result at 7.5 K is also consistent with the previous neutron diffraction experiment [7]. They reported the spin modes of Cr^{3+} are G_{xy} at 4.2K and G_x at 80K. The G_{xy} can be realized by the mixture of two phases from Γ_1 $(G_y; C_z^{Er})$ and Γ_4 $(G_x; F_z^{Er})$ like in Fig. 2 in the middle. No incommensurate peaks are observed in this case of $ErCrO_3$ down to $T = 5.0$ K. The incommensurate peaks, if present like in $DyFeO_3$ [30], would appear at (001) $\pm k$ as a pair, near the 2θ position of (001) reflection as indicated in Fig. 1.

TABLE III. Magnetic structure of $ErCrO_3$ at $T = 5$ K. The *R*-factors are $R_{\text{nuclear}} = 4.652\%$ and $R_{\Gamma_4} = 5.259\%$ with $\chi^2 = 3.17$. The symmetry permits the presence m_a and m_c components for Cr, but according to the best fit model, both m_a and m_c should ideally be zero. The symmetry of magnetic structure is Γ_1 $(G_y; C_z^R)$.

Atom		Atomic position	m_a	m_b	m_c	m_{total}
Er(1)	4*c*	$(x, y, 0.25)$	0	0	5.37(2)	5.37(2)
Er(2)		$(-x, -y, 0.75)$	0	0	5.37(2)	5.37(2)
Er(3)		$(x + 0.5, 0.5 - y, 0.75)$	0	0	−5.37(2)	5.37(2)
Er(4)		$(0.5 - x, 0.5 + y, 0.25)$	0	0	−5.37(2)	5.37(2)
Cr(1)	4*b*	$(0.5, 0, 0)$	0	2.55(3)	0	2.55(3)
Cr(2)		$(0.5, 0, 0.5)$	0	−2.55(3)	0	2.55(3)
Cr(3)		$(0, 0.5, 0.5)$	0	2.55(3)	0	2.55(3)
Cr(4)		$(0, 0.5, 0)$	0	−2.55(3)	0	2.55(3)

IV. THE NEUTRON ELASTIC SCATTERING ON THE SINGLE CRYSTAL OF $ErCrO_3$

To investigate the magnetic structure of $ErCrO_3$ in further detail, we performed neutron elastic scattering of the temperature dependence of these representative Bragg peaks by using the single-crystal sample. These five peaks (100), (101), (010), (011), and (110) are taken to determine the magnetic structure uniquely as shown in Fig. 3. The (101) and (011) appear when the Cr sublattice orders. A nonzero intensity intensifies in the reflections of (100) and (010) means the *R* sublattice ordering or a *C*-type configuration of Cr^{3+} ordering [5]. The (110) peak represents the ferromagnetic component along the c axis from either Er^{3+}, Cr^{3+}, or both ions. Figure 3(a) shows the temperature dependence of the (101) and (100) peaks. The (101) showed the $T_N = 133.2(1)$ K and another transition shown at (101) and (100) at $T_{SR} = 10.230(3)$ K. The intensities are fit by $I = I_0(1 - T/T_N)^{2\beta}$. The critical exponents are $\beta_{T_N} = 0.190(2)$ and $\beta_{T_{SR}} = 0.139(2)$. Figure 3(b) is, on the other hand, the temperature dependence of the (010) and (011) peaks. The peak (010) appears at $T_{SR} = 9.99(2)$ K and the (110) appears at $T_N = 132.0(1)$ K. These (100) and (010) only appear at 10 K where spin reorientation occurs. The (101)

TABLE IV. Magnetic structure of $ErCrO_3$ at $T = 7.5$ K. The R factors are $R_{\text{nuclear}} = 3.07\%$, $R_{\Gamma_4} = 10.3\%$ and $R_{\Gamma_1} = 7.29\%$ with $\chi^2 = 2.38$. The symmetries of the magnetic structure are Γ_4 $(G_x; F_z^R)$ and Γ_1 $(G_y; C_z^R)$.

Atom		Atomic position	m_a	m_b	m_c	m_{total}
Er(1)	4c	$(x, y, 0.25)$	0	0	2.03(3)	2.03(3)
Er(2)		$(-x, -y, 0.75)$	0	0	2.03(3)	2.03(3)
Er(3)		$(x + 0.5, 0.5 - y, 0.75)$	0	0	2.03(3)	2.03(3)
Er(4)		$(0.5 - x, 0.5 + y, 0.25)$	0	0	2.03(3)	2.03(3)
Cr(1)	4b	(0.5, 0, 0)	1.22(8)	0	0	1.22(8)
Cr(2)		(0.5, 0, 0.5)	−1.22(8)	0	0	1.22(8)
Cr(3)		(0, 0.5, 0.5)	1.22(8)	0	0	1.22(8)
Cr(4)		(0, 0.5, 0)	−1.22(8)	0	0	1.22(8)
Er(1)	4c	$(x, y, 0.25)$	0	0	3.36(2)	3.36(2)
Er(2)		$(-x, -y, 0.75)$	0	0	3.36(2)	3.36(2)
Er(3)		$(x + 0.5, 0.5 - y, 0.75)$	0	0	−3.36(2)	3.36(2)
Er(4)		$(0.5 - x, 0.5 + y, 0.25)$	0	0	−3.36(2)	3.36(2)
Cr(1)	4b	(0.5, 0, 0)	0	2.21(4)	0	2.31(3)
Cr(2)		(0.5, 0, 0.5)	0	−2.21(4)	0	2.31(3)
Cr(3)		(0, 0.5, 0.5)	0	2.21(4)	0	2.31(3)
Cr(4)		(0, 0.5, 0)	0	−2.21(4)	0	2.31(3)

and (011) peaks also slightly enhanced at that temperature. As shown in previous powder neutron-diffraction data, the (110) is different from the other four peaks. The (110) peaks show no clear transition at $T_N \approx 133$ K, however, it gradually increases the intensity to $T_{\text{Top}} = 9.6$ K. The peak intensity drops around the $T_{\text{Bottom}} = 8.0$ K. The drop is much sharper than neutron powder diffraction data. There exists no mixing phase of Γ_1 and Γ_4. The calculated Bragg scattering intensities (Table VI) based on these magnetic structure at 5 K (Table III) and 25 K (Table V) are reproducing the Bragg scattering intensities from the single-crystal sample. In addition, the observed ratio of (011) and (101) at 2.3 K is ∼1.86 which supports the magnetic structure is Γ_1 $(G_y; C_z^R)$ rather than Γ_1 $(G_y; -C_z^R)$, the calculated intensity of Γ_1 $(G_y; -C_z^R)$ of I_{011}/I_{101} is ≈0.02. Interestingly, that was the opposite result reported by Shamir [5] but agrees with the result reported by Bertaut [7]. So we conclude that spin reorientation of $ErCrO_3$ is Γ_4 (G_x, F_z) to Γ_1 $(G_y; C_z^R)$. This is the critical information when we investigate these Cr^{3+}-Cr^{3+}, Er^{3+}-Cr^{3+}, and Er^{3+}-Er^{3+} interactions. The measurement of single crystals showed that $T_{SR} \sim T_{Er^{3+}}$. So far, our observations support $T_{Er^{3+}} = 9.3$ K by considering other measurements shown later. These $T_{Er^{3+}}$ and T_{SR} could be the same temperature but not necessarily. The right-hand panels of Fig. 3 show that $T_{SR} = T_{Er^{3+}} = 9.3 \approx 10$ K.

TABLE V. Magnetic structure of $ErCrO_3$ $T = 25$ K. The R factors are $R_{\text{nuclear}} = 4.55\%$, $R_{\Gamma_4} = 12.1\%$ with $\chi^2 = 2.10$. The symmetry of the magnetic structure is Γ_4 (G_x, A_y, F_z), however, along the m_b is too small to determine by neutron diffraction.

Atom		Atomic position	m_a	m_b	m_c	m_{total}
Cr(1)	4b	(0.5, 0, 0)	2.44(2)	0	1.26(4)	2.75(4)
Cr(2)		(0.5, 0, 0.5)	−2.44(2)	0	1.26(4)	2.75(4)
Cr(3)		(0, 0.5, 0.5)	2.44(2)	0	1.26(4)	2.75(4)
Cr(4)		(0, 0.5, 0)	−2.44(2)	0	1.26(4)	2.75(4)

V. MAGNETIZATION OF $ErCrO_3$

The magnetic field was applied along all principal axes a, b, and c of the single-crystal sample with $H = 0.01$ T (Fig. 4). A weak ferromagnetic phase appears at $T = 133$ K in magnetization data with field along the c axis. The Cr^{3+} magnetic moment increases further upon cooling. Compared with the magnetization along the c axis, the moments along the a and b axes are negligible. The magnetization becomes flat at around $T \approx 30$ K, then a sharp drop of magnetic moment is observed at $T_{Er^{3+}} = 9.3$ K. The magnetization along the c axis starts to decrease at that temperature. The results are consistent with other single-crystal studies [14], but not with the studies with polycrystalline samples [12,13].

Figure 5 shows magnetic-field dependence of magnetization (M-H) of $ErCrO_3$ along all principal axes, a, b, and c directions of the single-crystal sample. A small magnetic hysteresis loop appears in the M-H curve [Fig. 5(b)] along the c axis. The magnetization along the b and c axes is easier to induce by applying a magnetic field, and the a axis is the hardest axis to force the magnetic moment to align parallel to the

TABLE VI. Calculated Bragg-peak intensities of Γ_1 at 5 K, Γ_4 at 25 K, and $\Gamma_1 + \Gamma_4$ at 7.5 K based on the determined magnetic structures as shown in Tables III to V. The calculation supports both single-crystal and powder diffraction data.

Bragg peaks	I_N	I_M	$I_{25\,\text{K}}$	I_M	$I_{7.5\,\text{K}}$	I_M	$I_{5\,\text{K}}$
(001)	0	0	0	0	0	0	0
(010)	0	0	0	10.6	10.6	27.0	27.0
(100)	0	0	0	12.8	12.8	32.5	32.5
(011)	0	6.72	6.72	8.73	8.73	12.7	12.7
(101)	0.16	2.20	2.36	6.26	6.42	7.33	7.49
(110)	0.01	1.79	1.80	4.53	4.54	0.08	0.09
(002)	0.15	0	0.15	0	0.15	0	0.15
(020)	3.33	1.75	5.08	1.87	5.10	0	3.33
(200)	2.33	1.75	4.08	4.33	6.66	0	2.33

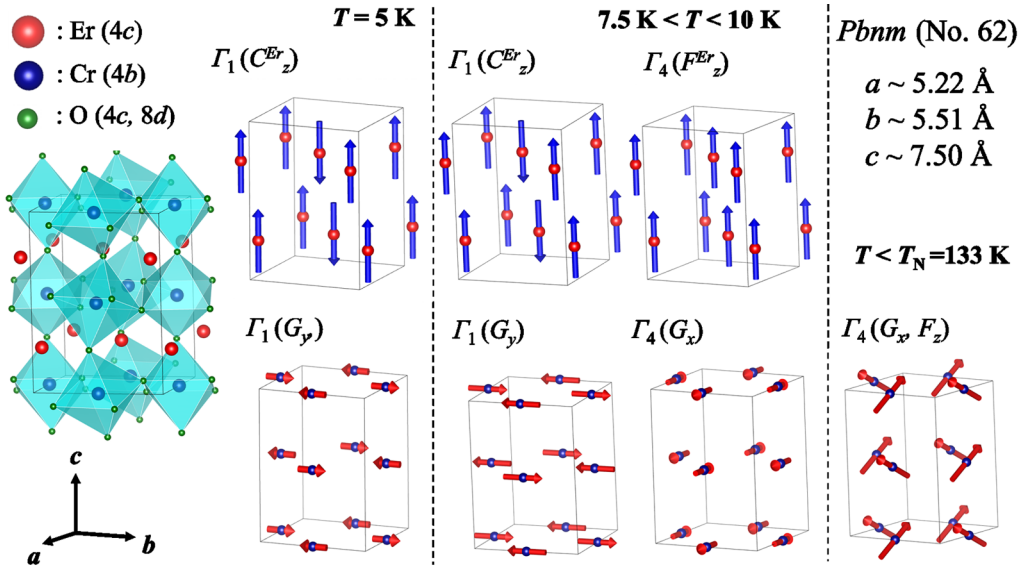

FIG. 2. The crystal and magnetic structures of $ErCrO_3$.

magnetic field. Antiferromagnetic order of Er^{3+} prevents magnetic moment alignment along the magnetic field in the b and c axes. With increasing temperature, that effect has been weakening. The magnetic moment becomes easier to align along the magnetic field at 15 K where only the Cr^{3+} ions order.

VI. SPECIFIC HEAT OF $ErCrO_3$

To clarify the transition of this $ErCrO_3$ single-crystal, the specific-heat measurements were performed in both polycrystalline and single-crystal samples (Fig. 6). For the single-crystal sample, the magnetic field was applied along the c axis.

The specific heat shows two clear first-order transitions at $T = 133$ and 9.3 K, respectively. For the peak at the higher temperature, the transition temperature $T_N = 133$ K, which is consistent with magnetization and other experimental results. The second sharp transition is at $T = 9.3$ K. The transition supports the Er order at that temperature. Below $T = 9.3$ K, there are Schottky anomalies for both single-crystal and polycrystalline samples. The polycrystalline specific-heat data shows no transition at $T \approx 10$ K while the single crystal shows a sharp peak with the maximum appearing at $T = 9.3$ K. No peak was detected in the 15 to 30 K regimes. Upon applying a magnetic field $H = 5.0$ T, the Schottky anomaly disappears. Estimated energy gaps are $\Delta = 13.23(3)$ K in

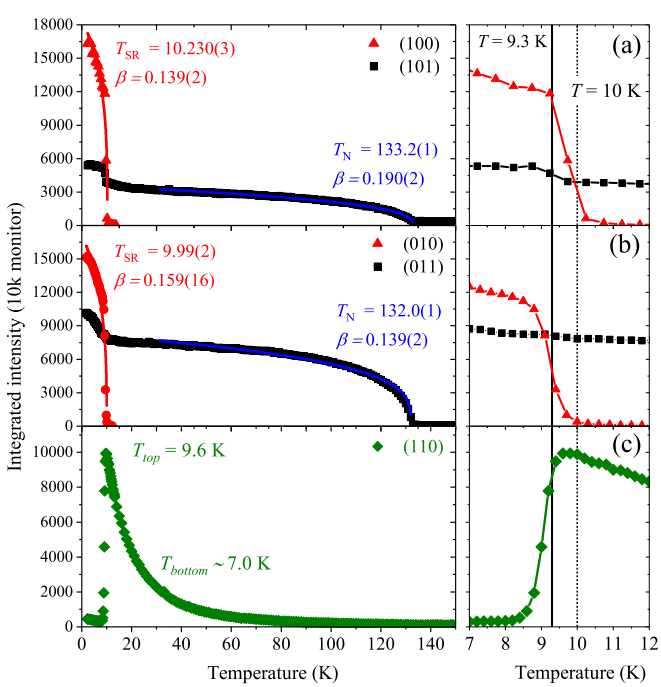

FIG. 3. Temperature dependence of Bragg peak intensities (101), (100), (010), (011), and (110) of the single crystal $ErCrO_3$.

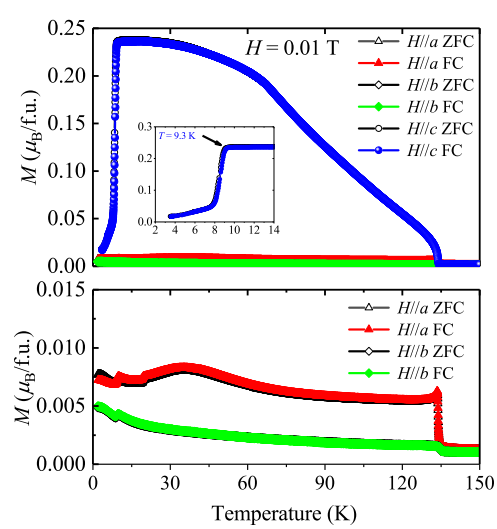

FIG. 4. Temperature dependence of magnetization of $ErCrO_3$. The measurement has been done by applying a magnetic field for each crystal axis with $H = 0.01$ T.

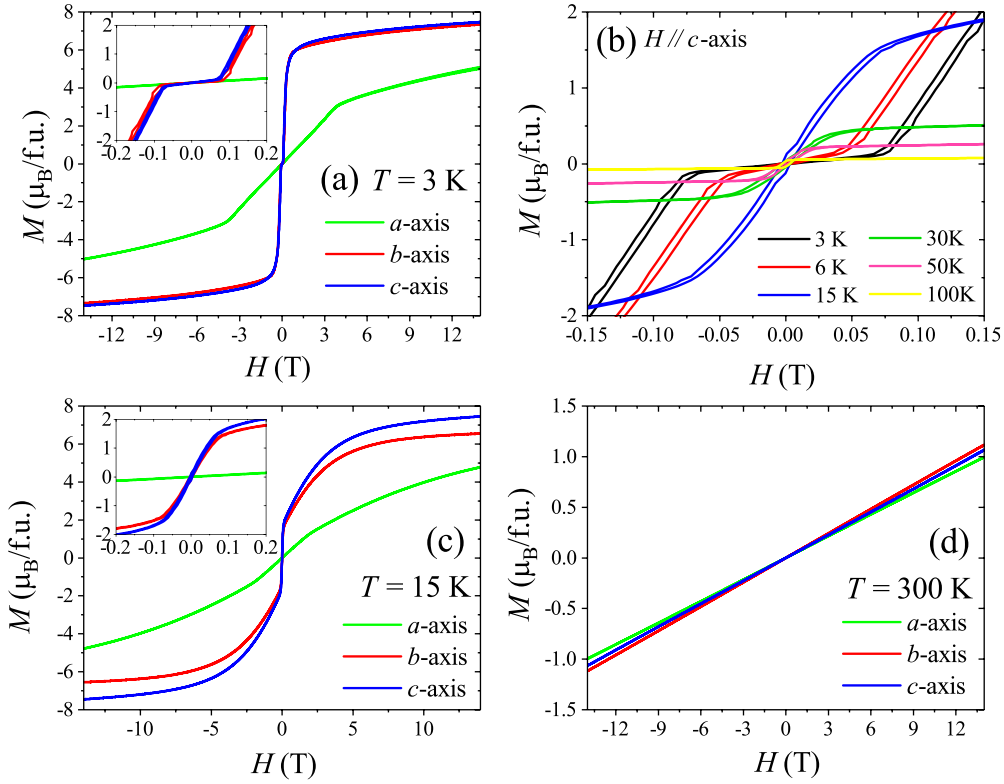

FIG. 5. Magnetic-field dependence of magnetization of $ErCrO_3$ at various temperatures. The measurement has been done for the single-crystal sample by applying a magnetic field for each crystal axis. The insets indicated the difference on the M-H curve below $T_{Er^{3+}}$ and above $T_{Er^{3+}}$ at low magnetic-field region.

single-crystal and $\Delta = 12.90(4)$ K in polycrystalline samples. We attribute these to the lowest crystal-field level from the ground $^4I_{15/2}$ of the Er^{3+} ions.

VII. CRYSTAL-FIELD EXCITATIONS OF $ErCrO_3$

Inelastic neutron scattering was performed on a single-crystal sample. The constant-Q scans at $Q = (0.8\,0\,0)$ at various temperatures were implemented. The instrument energy resolution is about $\Delta E \approx 0.15$ meV. We observed the crystal-field excitation of $^4I_{15/2}$ from Er^{3+}. Figure 7 shows that the crystal-field excitation of Er^{3+} is estimated to be 1.19(1) meV (13.80 K). The energy scale is close to the Schottky anomaly obtained from the specific-heat data and the peak of excitation disappears at 12 K. The lowest crystal-field excitation Er^{3+} in isostructural $ErFeO_3$ shows a giant shift from 0.3 to 0.8 meV by reducing temperature below $T_{Er^{3+}} =$ 4.1 K. O'Brien *et al.* modeled that excitation as the first Kramers doublet above the grand state $^4I_{15/2}$ of the Er^{3+} [31]. The Er^{3+} orders at 4.1 K in $ErFeO_3$ while the Er^{3+}

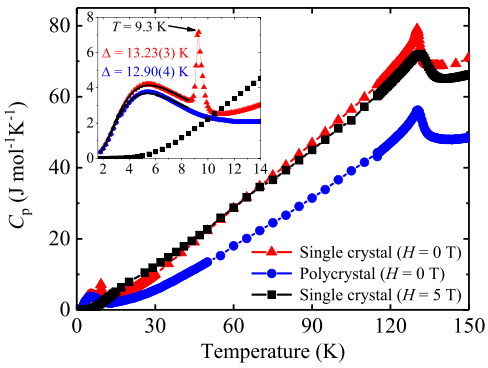

FIG. 6. The specific-heat data for polycrystalline and single-crystal samples $ErCrO_3$. The measurement has been done for the single crystal under $H = 0$ and 5.0 T and polycrystalline only under $H = 0$ T. Inset figure focuses on the low-temperature regime and the fitting to the Schottky anomaly.

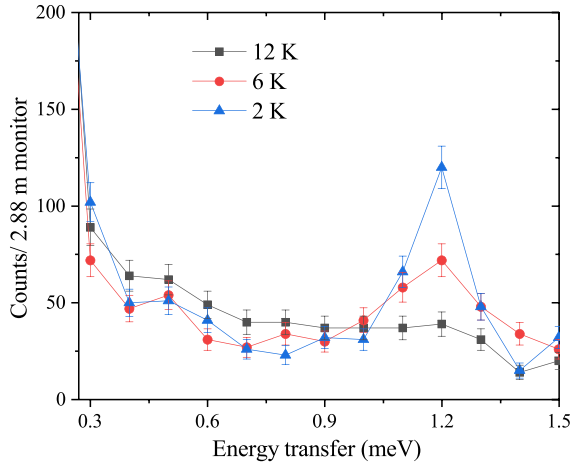

FIG. 7. The observed crystal-field excitations through inelastic neutron scattering.

TABLE VII. Magnetic phase-transition temperatures of $ErCrO_3$, $ErFeO_3$, and $ErAlO_3$.

	T_{SR} (K)	Spin reorientation	$T_{Er^{3+}}$	$T_{N^{Cr,Fe}}$	Ref.
$ErCrO_3$	9.3 ∼ 10	Γ_4 (G_x, F_z) to Γ_1 (G_y, C_z^R)	9.3	133	This work
$ErFeO_3$	87∼97	Γ_4 (G_x, A_y, F_z) to Γ_2 (F_x, C_y, G_z)	4.4	640	[32]
$ErAlO_3$			0.6		[33]

orders in $ErCrO_3$ at $T = 9.3$ K. Interestingly, the Er^{3+} orders antiferromagnetically at 0.6 K in $ErAlO_3$. The crystal-field excitation has been observed at 1.2 meV in $ErCrO_3$ and no clear energy shift by changing the temperature below and above $T_{Er^{3+}}$ unlike the case in $ErFeO_3$ [31].

VIII. DISCUSSION

In the rare-earth orthochromites and orthoferrites, magnetic interactions R^{3+}-R^{3+}, R^{3+}-(Cr, Fe)$^{3+}$, and (Cr, Fe)$^{3+}$-(Cr, Fe)$^{3+}$ can coexist to establish such variety of magnetic structures and phase transitions.

The systematic investigation of both powders and single crystals of $ErCrO_3$ has been performed. The neutron powder diffraction showed a mixing phase of Γ_1 (G_y, C_z^R) and Γ_4 (G_x, F_z^R). Note that neutron powder diffraction data cannot distinguish the combination of the two irreducible representations from the phase coexistence of two different irreducible representations. The polycrystalline samples have the tendency to accommodate defects and vacancies at their grain boundaries [13,26]. These magnetic interactions of R^{3+}-R^{3+}, R^{3+}-Cr^{3+}, and Cr^{3+}-Cr^{3+} in the single crystal should be able to spread over the sample more easily than in the polycrystalline sample. Especially, the ferroelectric ordering reported in $RCrO_3$ in polycrystalline samples, however, the homogeneous ferroelectric ordering in the single-crystal sample has not been detected [13,22,26,27]. The previous reports [22,27] show that there is a local polar domain from impurities from (i) Bi^{3+} or (ii) Pb^{2+} or Pb^{4+}, which are likely formed through the spontaneous crystallization in the solution-melt. We have grown the single crystal by the floating zone method so there is no (i) Bi^{3+} or (ii) Pb^{2+} or Pb^{4+} in the sample-making process. Our single crystals are good candidates to investigate ferroelectric ordering.

Spin reorientation of Cr^{3+} and Er^{3+} order temperature are not necessarily the same. For example, isostructural $ErFeO_3$ has $T_{Er^{3+}} = 4.4$ K, $T_{SR} = 87$–97 K, and $T_N = 640$ K, where interactions between the Fe^{3+} are stronger [32]. The spin reorientation transition of $ErCrO_3$ is still sharper compared with the $ErFeO_3$ [32], which occurs over a range of 11 K. In another isostructural $ErAlO_3$, the Er^{3+} orders antiferromagnetically at 0.6 K [33]. These different isostructural $ErFeO_3$, $ErCrO_3$, $ErAlO_3$ compounds show the difficulty of understanding magnetic interactions R^{3+}-R^{3+}, R^{3+}-(Cr, Fe)$^{3+}$, and (Cr, Fe)$^{3+}$-(Cr, Fe)$^{3+}$ of this system and it needs to be investigated further. Neutron elastic scans for Bragg peaks clearly identified the spin reorientation of Cr^{3+} showing that (110) peak intensity dropped below $T = 9.6$ K just above the $T_{Er^{3+}}$. Yamaguchi *et al.* have shown that the anisotropic parts of the magnetic interactions of R^{3+}-Cr^{3+} are generally responsible for the spin reorientation [34]. In the case of $ErCrO_3$, the energy scales of these Er^{3+}-Er^{3+} and Er^{3+}-Cr^{3+} interactions are close to each other because $T_{Er^{3+}}$ and T_{SR} are almost the same temperature. The counterpart $ErFeO_3$ is another interesting material [35]. Transition temperatures are at $T_{Er} = 4.4$ K, $T_{SR} = 87$–97 K and $T_N = 640$ K. The spin reorientation occurs over a range of 11 K [32], the change is gradual, that is different from what we observed in $ErCrO_3$. Both Er orthochromite and orthoferrite show Er^{3+} order with C_z under their $T_{Er^{3+}}$. In general, interactions of Fe^{3+}-Fe^{3+} are stronger than those of Cr^{3+}-Cr^{3+}, where we observed higher T_{SR} and T_N in $RFeO_3$. $ErAlO_3$ shows importance of understanding of magnetic interactions R^{3+}-R^{3+}, R^{3+}-(Cr,Fe)$^{3+}$, and (Cr,Fe)$^{3+}$-(Cr,Fe)$^{3+}$ of this system. Since Al is a nonmagnetic atom, the magnetic interaction is assumed to be Er^{3+}-Er^{3+}. The magnetic phase transition reported is at 0.6 K [33]. The Er^{3+}-Er^{3+} interaction is supposed to cause the Er^{3+} order, so being $T_{Er^{3+}} = 4.4$ K on $ErFeO_3$, $T_{Er^{3+}} = 9.3$ K on $ErCrO_3$, there should be the other two interactions establishing the ordering at these temperatures. The T_{SR}, $T_{Er^{3+}}$ and T_N are summarized in Table VII.

Crystal-field excitation and specific-heat measurements show that the lowest-lying Kramers doublets of $^4I_{15/2}$ are $\Delta = 13.23(3)$ K from the specific-heat measurement and $\Delta = 1.19(1)$ meV $= 13.80(1)$ K from the crystal-field excitation. A shift of the energy of the lowest crystal-field excitation of $^4I_{15/2}$ of Er^{3+} has been observed in $ErFeO_3$ at $T_{Er^{3+}}$. There is no such shift observed in the case of $ErCrO_3$. In addition, by fitting the external magnetic-field dependence of the crystal-field excitation energy, the internal field of Er^{3+} magnetic moment was derived to be 0.33 meV in $ErFeO_3$ [31]. That internal field of Er^{3+} magnetic moment does not appear in $ErCrO_3$. The slightly dispersive crystal field excitations were observed in $ErFeO_3$ [36] due to the exchange of the Er^{3+} and Fe^{3+}. It would be interesting to investigate that phenomena in $ErCrO_3$, however, the sample was only 0.67 grams, and it was still too small to perform Q dependence and temperature dependence of crystal-field excitations within a reasonable neutron beam time. The Er^{3+} ordering temperature in $ErCrO_3$ is at least two times higher than that of $ErFeO_3$. The Er^{3+} orders antiferromagnetically at 0.6 K in $ErAlO_3$ and Er^{3+}-Er^{3+} interaction should be similar in $ErFeO_3$, $ErCrO_3$, and $ErAlO_3$. In addition, the magnetic interactions in Fe^{3+}-Fe^{3+} are much stronger than that of Cr^{3+}-Cr^{3+}, the magnetic interactions R^{3+}-(Cr or Fe)$^{3+}$ is a key to understand the Er^{3+} ordering temperature and spin reorientation of $ErCrO_3$. As shown above, T_{SR} and $T_{Er^{3+}}$ are very close in $ErCrO_3$. These magnetic interactions Er^{3+}-Er^{3+} and Cr^{3+}-Er^{3+} should have a similar energy scale. That could make the $ErCrO_3$ rare and important material among orthoferrite and orthochromite for applications especially when Er^{3+} or Cr^{3+} are selectively excited through lasers. The magnetic excitations of $ErCrO_3$ are still needed to investigate in detail to understand this system. Especially, the orthochromites are less studied and no magnetic

excitations have been reported so far. Large single-crystal samples without impurities are now in preparation, inelastic neutron scattering will reveal more to investigate in detail of these interactions.

IX. SUMMARY

$ErCrO_3$ has been investigated via neutron-scattering techniques, magnetization measurement, and specific-heat measurement using single-crystal and polycrystalline samples. Neutron powder diffraction shows a mixing phase of Γ_1 (G_y, C_z^R) and Γ_4 $(G_x; F_z^R)$ just below $T = 10$ K while single-crystal neutron elastic-scattering experiments show the transition in a very narrow range. The results indicate the size of the crystal affects the stability of the magnetic phase, which could explain the inconsistency of magnetic transition temperature and magnetic structure reported so far. Based on the measurements on the single crystal by neutron scattering, magnetization, and specific heat, we conclude the $T_N = 133$ K, $T_{SR} = T_{Er^{3+}} = 9.3$ K. The temperatures are important when magnetic phase or magnetic atoms are manipulated by physical parameters, such as a magnetic or optical field. The specific heat and neutron inelastic scattering reveal that the low-lying crystal-field excitation of the first Kramers doublet above the grand state $^4I_{15/2}$ of the Er^{3+} in $ErCrO_3$ is $\Delta \approx 13.2$ K, which is at least two times higher than that of the Er^{3+} in $ErFeO_3$. These magnetic interactions Er^{3+}-Er^{3+} and Cr^{3+}-Er^{3+} are similar energy scale in $ErCrO_3$. $ErCrO_3$ could be an important material for application among these orthoferrites and orthochromites.

ACKNOWLEDGMENTS

Financial support for the neutron-scattering instrument Sika from the Ministry of Science and Technology, Taiwan (Grant No. MOST 109-2739-M-213-001) is gratefully acknowledged. S.Y. was financially supported by the Ministry of Science and Technology, Taiwan (Grants No. 110-2112-M-213-013, No. 111-2112-M-213-023, and No. 112-2112-M-213-019). The work at the University of Macau was supported by the Science and Technology Development Fund, Macao SAR (Files No. 0090/2021/A2 and No. 0049/2021/AGJ) and University of Macau (MYRG2020-00278-IAPME). The experiments were performed under the ANSTO user program with Proposals No. P13966 (Sika) and No. MI13435 (Echidna).

[1] M. Imada, A. Fujimori, and Y. Tokura, Rev. Mod. Phys. **70**, 1039 (1998).
[2] J. M. D. Coey, M. Viret, and S. von Molnar, Adv. Phys. **48**, 167 (1999).
[3] U. Chowdhury, S. Goswami, D. Bhattacharya, J. Ghosh, S. Basu, and S. Neogi, Appl. Phys. Lett. **105**, 052911 (2014).
[4] B. Tiwari, M. K. Surendra, and M. S. Ramachandra Rao, Mater. Res. Express **1**, 036102 (2014).
[5] N. Shamir, H. Shaked, and S. Shtrikman, Phys. Rev. B **24**, 6642 (1981).
[6] E. Bousquet and A. Cano, J. Phys.: Condens. Matter **28**, 123001 (2016).
[7] E. F. Bertaut, G. Bassi, G. Buisson, P. Burlet, J. Chappert, A. Delapalme, J. Mareschal, G. Roult, R. Aleonard, R. Pauthenet, and J. P. Rebouillat, J. Appl. Phys. **37**, 1038 (1966).
[8] K. Tezuka, Y. H. A. Nakamura, T. Inami, Y. Shimojo, and Y. Morii, J. Solid State Chem. **141**, 404 (1998).
[9] S. Miyoshi, S. Onuma, A. Kaimai, H. Matsumoto, K. Yashiro, T. Kawada, J. Mizusaki, and H. Yokokawa, J. Solid State Chem. **177**, 4112 (2004).
[10] S. Mahana, U. Manju, and D. Topwal, J. Phys. D: Appl. Phys. **51**, 305002 (2018).
[11] H. Das and A. F. Rébola, and T. Saha-Dasgupta, Phys. Rev. Mater. **5**, 124416 (2021).
[12] Y. Su, J. Zhang, B. Li, B. Kang, Q. Yu, C. Jing, and S. Cao, Appl. Phys. A **100**, 73 (2010); Ceram. Int. **38**, S421 (2012).
[13] B. Rajeswaran, D. I. Khomskii, A. K. Zvezdin, and C. N. R. Rao, and A. Sundaresan, Phys. Rev. B **86**, 214409 (2012).
[14] L. H. Yin, J. Yang, P. Tong, X. Luo, C. B. Park, K. W. Shin, W. H. Song, J. M. Dai, K. H. Kim, X. B. Zhu, and Y. P. Sun, J. Mater. Chem. C **4**, 11198 (2016).
[15] T. Kitazono, I. Umehara, and T. Sekiya, J. Phys. Soc. Jpn. **76**, 112 (2007).
[16] Y. Zhu, J. Xia, S. Wu, K. Sun, Y. Yang, Y. Zhao, H. W. Kan, Y. Zhang, L. Wang, H. Wang, J. Fang, C. Wang, T. Wu, Y. Shi, J. Yu, R. Zhang, and H.-F. Li, iScience **25**, 104111 (2022).
[17] M. Kaneko, S. Kurita, and K. Tsushima, J. Phys. C: Solid State Phys. **10**, 1979 (1977).
[18] K. Toyokawa, S. Kurita, and K. Tsushima, Phys. Rev. B **19**, 274 (1979).
[19] A. Hasson, R. M. Hornreich, Y. Komet, B. M. Wanklyn, and I. Yaeger, Phys. Rev. B **12**, 5051 (1975).
[20] R. S. Meltzer and H. W. Moos, J. Appl. Phys. **41**, 1240 (1970).
[21] E. F. Bertaut and J. Mareschal, Solid State Commun. **5**, 93 (1967).
[22] V. A. Sanina, B. K. Khannanov, E. I. Golovenchits, and M. P. Shcheglov, Phys. Solid State **61**, 370 (2019).
[23] M. Eibschütz, L. Holmes, J. P. Maita, and L. G. Van Uitert, Solid State Commun. **8**, 1815 (1970).
[24] L. Holmes, M. Eibschütz, and L. G. Van Uitert, J. Appl. Phys. **41**, 1184 (1970).
[25] S. Kurita, Y. Tazaka, and K. Tsushima, J. Phys. Soc. Jpn. **56**, 612 (1987).
[26] K. R. S. Preethi Meher, A. Wahl, A. Maignan, C. Martin, and O. I. Lebedev, Phys. Rev. B **89**, 144401 (2014).
[27] V. A. Sanina, B. K. Khannanov, E. I. Golovenchits, and M. P. Shcheglovl, Phys. Solid State **60**, 2532 (2018).
[28] M. Avdeev and J. R. Hester, Echidna: A decade of high-resolution neutron powder diffraction at OPAL, J. Appl. Crystallogr. **51**, 1597 (2018).
[29] C.-M. Wu, G. Deng, J. S. Gardner, P. Vorderwisch, W.-H. Li, S. Yano, J.-C. Peng, and E. Imamovic, J. Instrum. **11**, P10009 (2016).
[30] C. Ritter, R. Vilarinho, J. A. Moreira, M. Mihalik, M. Mihalik, and S. Savvin, J. Phys.: Condens. Matter **34**, 265801 (2022).

[31] J. O'Brien and C. Ulrich (private communication).
[32] H. Pinto, G. Shachar, H. Shaked, and S. Shtrikman, Phys. Rev. B **3**, 3861 (1971).
[33] J. Sivardiere and S. Quuezel-ambrunaz, C. R. Acad. Sci. Paris **273**, 619 (1971).
[34] T. Yamaguchi, J. Phys. Chem. Solids **35**, 479 (1974).
[35] D. G. Oh, J. H. Kim, H. J. Shin, Y. J. Choi, and N. Lee, Sci. Rep. **10**, 11825 (2020).
[36] M. P. Zic, W. T. Fuhrman, K. Wang, S. Ran, and J. Paglione, J. Appl. Phys. **130**, 014102 (2021).